Asymmetric Stark shift in $Al_xIn_{1-x}As/Al_yGa_{1-y}As$ self-assembled dots

S. Raymond, J. P. Reynolds, and J. L. Merz
Department of Electrical Engineering, University of Notre Dame, Notre Dame, Indiana 46556

S. Fafard, Y. Feng, and S. Charbonneau
Institute for Microstructural Sciences, National Research Council, Ottawa, Ontario, Canada K1A 0R6

(Received 26 June 1998)

We present microphotoluminescence measurements of self-assembled quantum dots subject to an electric field applied along the growth axis. The spectra reveal sharp peaks corresponding to a number of ''single-dot'' emission lines. An asymmetric Stark shift as a function of applied field is obtained; for positive fields (electron pushed towards the apex of the dot), an initial blueshift is measured, followed by saturation and eventually a small redshift for stronger positive fields, while a continuous redshift is observed for negative field values. High positive fields also give rise to structural changes in the emission spectra as lines are enhanced or quenched under the influence of the field. The field dependence of the emission lines are reproduced in our theoretical calculations, which show that the asymmetric Stark shift is caused by the combination of dot geometry and strong lateral confinement. [S0163-1829(98)53144-X]

The zero-dimensional (0D) properties of self-assembled dots, both physical and electronic, have now been evidenced in a number of different experiments. In particular, ''single-dot'' emission was obtained by performing microluminescence experiments to probe a finite number (few hundred) of dots.[1–3] Some studies have also focused on the Coulomb interactions between carriers trapped in the same dot[4–6] or between carriers in neighboring dots.[7–9] As a first step in understanding coupling among multiple dots we investigate the electronic properties of single excitons trapped within individual quantum dots. Specifically, we report on the effect an electric field has upon luminescence when applied along the growth axis of individual $In_{0.64}Al_{0.36}As$ self-assembled dots. The few dot spectrum is obtained by performing microphotoluminescence (μPL) measurements and focusing on a narrow energy range. Individual emission peaks show an asymmetric Stark shift as a function of applied field. Results from our theoretical modeling indicate that this asymmetry arises from the geometry of the quantum dot's confinement potential along the growth axis.

The sample was grown by molecular beam epitaxy (MBE) on an *n*-doped substrate. After deposition of a 20 nm doped ($n=10^{18}$) GaAs buffer layer, a five-period $Al_{0.5}Ga_{0.5}As/GaAs$ superlattice smoothing structure was grown. The remaining layers were then grown as follows: 500 nm ($n=10^{18}$) GaAs back contact layer, 10 nm nonintentionally doped (nid) spacer layer, 250 nm nid $Al_{0.3}Ga_{0.7}As$ barrier layer, 1.3 nm $In_{0.64}Al_{0.36}As$ nid quantum-dot (QD) layer, 250 nm nid $Al_{0.3}Ga_{0.7}As$ barrier layer, 10 nm nid GaAs spacer layer, and finally 190 nm ($n=10^{18}$) GaAs top contact layer. The resulting quantum dots have a base diameter of approximately 19 nm with a thickness of 3.4 nm and an areal density of 20 μm^{-2}. The sample was processed into several square mesas of different sizes, with the surrounding sample etched down to approximately midway into the doped GaAs back contact layer. Figure 1 shows the cross section of one of the resulting mesas, where the top of the mesa is covered with SiO_2 except for a circular opening allowing a gold layer to contact the surface of the sample. A small window, 3 μm in diameter, is opened in the gold so as to perform μPL experiments and probe a limited number of dots ($\sim$140). Since the intrinsic $Al_yGa_{1-y}As$ barriers on each side of the QD region are highly resistive compared to other regions of the sample, the voltage drop occurs nearly entirely within this center intrinsic region. Moreover, since the electrical current flowing in the sample is negligible, net charges are going to accumulate on both sides of the intrinsic region, not within it. This implies a constant electric field in this barrier-dot-barrier region, which can be calculated from the simple expression $F=V/l$ where F is the constant field, V is the applied voltage, and l is the thickness of the intrinsic region ($l\approx$500 nm). From the sample geometry, the field is oriented

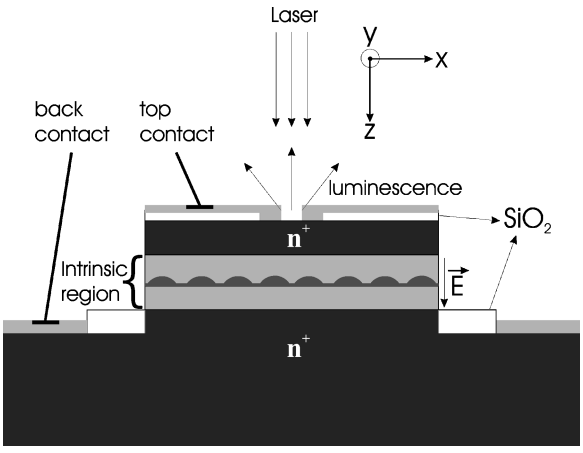

FIG. 1. Example of the mesa design used to apply a known electric field to a self-assembled dot layer. The sample was etched down to the n^+ buffer layer to define square mesas (in this case 80 μm in size) on the sample surface. SiO_2 was used to insure good electrical isolation and to limit the risk of spiking. A top (back) ohmic contact is formed by diffusing Au/Ge in the cap layer (n^+ buffer layer). A 3 μm window is opened in the top contact for laser excitation and light collection.

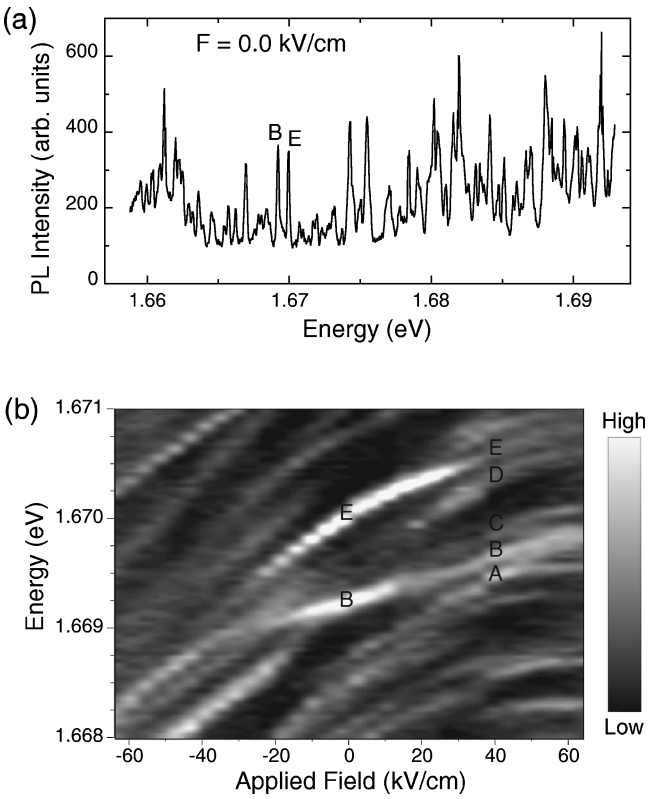

FIG. 2. (a) Low temperature (5 K) photoluminescence spectrum collected from the 3 μm window at zero applied field. (b) Greyscale density plot of the emission intensity in a narrow spectral range as a function of applied field. A few peaks have been labeled for discussion. All of the emission lines can be seen to shift asymmetrically as a function of applied field strength. The relative intensity of individual peaks also changes as the field is tuned.

along the z axis (growth direction) perpendicular to the base of the dots in the x-y plane. The field is taken positive when the field lines point from top to substrate.

The photoluminescence (PL) experiments were performed using a continuous wave Ar^+-ion pumped dye laser system with the tuned at a wavelength of 639.8 nm. The excitation power density at the sample surface was kept low ($\sim$35 W/cm^2) such that each dot is occupied on average by less than one electron-hole pair. The PL emitted from the dots was collected and focused on the entrance slits of a 0.64 m spectrometer with a single grating of 1800 g/mm, and detected by a liquid-nitrogen cooled charge coupled device (CCD) detector. PL lines as sharp as 90 μeV could be resolved with this system.

Figure 2(a) shows the results obtained at zero applied field for a square mesa of 80 μm sides with a top opening of 3 μm in diameter. The μPL reveals a number of ultrasharp lines corresponding to ''single-dot'' emission lines originating from a number of different dots with varying sizes, composition, strain, etc. Note that the spectrum in Fig. 2(a) is restricted to an energy window ranging roughly from 1.66 to 1.693 eV, but similar results were obtained from energies ranging from 1.66 to 1.85 eV, with the strongest emission observed around 1.77 eV.

The μPL experiments were repeated for field-strength increments of 4 kV/cm in the range -64 to 64 kV/cm. For higher magnitudes of the field, the photoluminescence intensity decreases by a factor of at least 3 due to field-induced carrier diffusion away from the dot layer before trapping and recombination can occur. Figure 2(b) shows a greyscale density plot of emission line intensities as a function of emission energy and applied electric field. In the figure, the lighter shade corresponds to emission peaks, and the spectra at each field value have been renormalized so one can follow the emission peaks up to large field strengths. The energy range has been restricted from 1.668 eV to 1.671 eV in the figure so as to probe only a few dots. The two strongest peaks at 0 kV/cm are labeled B and E, respectively, and the corresponding peaks are also labeled in Fig. 2(a) for clarity.

The most striking feature in Fig. 2(b) is the asymmetric Stark shift seen in the emission energies as a function of applied electric field. For example, by following peaks B and E on the surface plot for increasing positive fields one observes a blueshift of the emission until reaching a maximum energy around 60 kV/cm. The spectra also clearly show that the emission is redshifted for negative applied fields. The same general trend is observed at all emission energies, but with variations in the curvature and position of the extrema. Some emission lines show a saturation of the blueshift at lower fields ($\sim$40 kV/cm) followed by a reversal to a redshift. These differences among the emission lines are likely related to variations in size, composition, etc. of individual quantum dots.

Let us discuss the origin of the observed asymmetric Stark shift. The emission energy of a single exciton confined in a quantum dot can be expressed as follows:

$$E = E_{\text{gap}} + E_e(F) + E_{HH}(F) - R(F)\,, \tag{1}$$

where E is the emission energy, $E_e(F)$ and $E_{HH}(F)$ are the field-dependent single-particle ground-state confinement energy for the electron and heavy hole, respectively, and $R(F)$ is the field-dependent exciton binding energy in the quantum dot. Due to the strong confinement of the exciton in the dot, $R(F)$ is expected to show little variation within the range of field strengths investigated, and its contribution to the emission energy is therefore neglected in our theoretical modeling.

In order to capture the essential physics of the problem, we model $E_e(F)$ and $E_{HH}(F)$ by casting the 3D problem into a 1D problem that accounts for the lateral confinement felt by the carriers as they move in the z direction. By assuming that the motion in the z direction can be separated from that of the x-y plane, one may approximate the potential in the z direction as a square well, $V_0(z)$, defined by the cross section of the quantum dot along the z axis at its thickest point. The effective potential, $V_{\text{eff}}(z)$, is formed by adding a z-dependent energy term, $E_{x\text{-}y}(z)$, which accounts for the increase in energy due to lateral confinement. Outside the well $E_{x\text{-}y}(z)$ is zero, while inside it is defined by the ground-state energy of the 2D cylindrical well of radius $\rho(z)$ [see Fig. 3(a)].[10] The resulting effective potentials are plotted as a function of z for both the hole and electron in the right portion of Fig. 3(a). One then adds an electric field term to the Hamiltonian and numerically computes[11] the electron and hole ground-state confinement energies for each value of the field needed [see inset of Fig. 3(b)]. Finally, the emission energies are found using Eq. (1). The resulting field dependence of the Stark shift is shown for three dots of differing

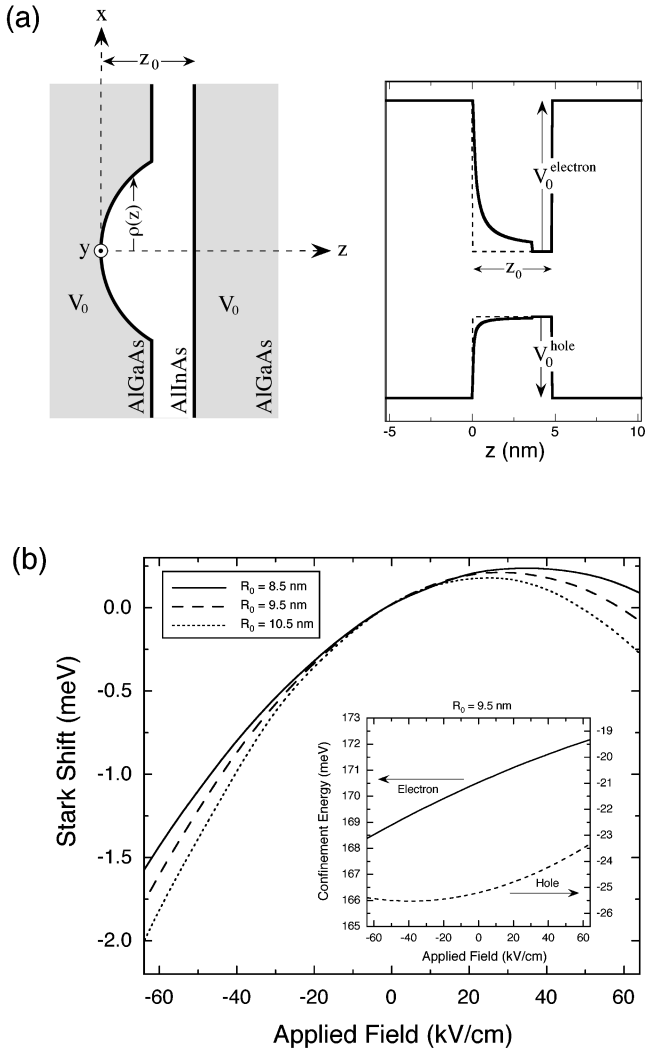

FIG. 3. (a) Assumed shape of a single dot and its corresponding effective 1D potential for the z direction. The modeled dots are chosen to have a base radius, R_0, of 8.5, 9.5, and 10.5 nm, and a height of 3.1, 3.5, and 3.9 nm, respectively. The wetting layer thickness is kept at a constant value of 1.2 nm. (b) Resulting Stark energy shifts for the three chosen dot sizes as a function of electric field strength applied along the z axis. The inset shows the electron and hole confinement energies for the $R_0 = 9.5$ nm dot.

size in Fig. 3(b);[13] one sees a blueshift for small positive fields, as well as a continuous redshift for negative field values. The magnitudes of the calculated shifts are consistent with the experimental values. The theoretical calculations show that the blueshift is mainly due to a strong increase in the electron confinement energy, as the field forces the electron towards the apex of the dot. Because absolute emission energies depend highly on an accurate estimate of E_{gap}, which is sensitive to stress, temperature, and accurate band parameters for $Al_xIn_{1-x}As$,[12] we find that our calculated emission energies fall below the experimental values by about 200 meV. However, the relative dependence of the emission energy on dot size can be accurately calculated. We find that a change in the base radius of the dot by 1 nm changes the absolute emission energy by approximately 20 meV. Estimates of the range in dot sizes would indicate a variation of emission energies on the order of 200 meV, in agreement with the full range of experimentally measured emission lines.

Other factors may play a role in the asymmetry observed, but evidence indicates that their influences are secondary to the geometric considerations discussed. For example, a contribution could originate from a built-in electric field within the sample which is progressively overcome by the applied field, thus causing an offset in the energy shifts. However, such a built-in field would contribute, as does the applied field, to a measured photocurrent in the range of microamperes as the laser is incident to the sample. No photocurrent could be detected at zero field, which indicates no built-in field is present in the sample. Another contribution could come from an electric field confined in or near the dots. This is possible if, for example, the strain present in the dots causes a strong piezoelectric effect. The presence of such fields in self-assembled dots was predicted by theoretical calculations that assume the dot is bound by crystallographic planes.[14] However, the magnitude of these piezoelectric fields is much less than that of the applied fields and thus this effect also should be small.

Another interesting field dependency that can be seen in Fig. 2(b) is that features appear and disappear in the spectrum as the field is tuned. For example, for 20 kV/cm and higher fields peak B is surrounded by peaks A and C, which could not be clearly identified at zero field. Likewise, feature D appears on the low-energy side of peak E, and one can also identify a feature appearing on its high-energy side. Also for lower negative fields, peak E disappears, while in the same range a feature on the low-energy side of peak B appears.

The variation in relative intensity of the emission lines for different ranges in the field's magnitude cannot be accounted for using our simple 1D energy models. This effect if probably related to the modification of the emission selection rules, which depends strongly upon the actual form of the field-dependent wave functions. We only note that the increased number of emission lines found at high positive fields could indicate the involvement of excited hole states, which become closely spaced in energy as the hole is forced into the less confining wetting layer. The new lines may also arguably originate from many-body effects arising when electron-hole pair annihilation occurs in the presence of other carriers. The diffusion of carriers created in the barrier material is affected by the presence of the electric field, causing a change in the probability of the carriers to become trapped in the QD layer. The resulting modification of the average dot population may enhance or quench emission lines associated with various excitonic complexes. The model used in this paper has neglected such many-body effects and it is likely that different excitonic complexes would be affected differently by the electric field. This could explain the different curvatures observed for various experimental emission lines, as well as discrepancies in this curvature between experiment and theory. However, the laser excitation intensity was intentionally kept at a level that should provide less than one electron-hole pair per dot on average, thus strongly limiting the influence of many-body effects in the system.

In conclusion, we have obtained μPL spectra of self-assembled dots as a function of electric field strength, and by focusing on a narrow energy range we were able to monitor the evolution of single-dot emission lines as a function of an externally applied electric field. An asymmetric Stark shift was observed in the emission energies with a blueshift for fields that push the electron towards the apex of the dot, and a redshift when the electron is forced towards the wetting layer. The asymmetric shift was reproduced using a 1D effective potential model, and in light of this calculation the blueshift is seen to be a result of the strong increase of the electron confinement energy as the electric field drives it towards the apex of the dot. The origin of the appearance and disappearance of some emission lines as the field is tuned is not yet well understood and this remains a topic of further investigations.

We would like to acknowledge our colleague A. M. Mintairov for his constructive comments and fruitful discussions.

[1] V. Nikitin, P. A. Crowell, J. A. Gupta, D. D. Awscalom, F. Flack, and N. Samarth, Appl. Phys. Lett. **71**, 1213 (1997).

[2] M. Grundmann, J. Christen, N. N. Lendentsov, J. Bohrer, D. Bimberg, S. S. Rustinov, P. Werner, U. Richter, U. Gosele, J. Heydenreich, V. M. Ustinov, A. Yu Egorov, A. E. Zhukov, P. S. Kop'ev, and Zh. I. Alferov, Phys. Rev. Lett. **74**, 4043 (1995).

[3] S. Fafard, R. Leon, D. Leonard, J. L. Merz, and P. M. Petroff, Phys. Rev. B **50**, 8086 (1994).

[4] A. Wojs and P. Hawrylak, Phys. Rev. B **51**, 10 880 (1995).

[5] U. Bockelmann, P. Roussignol, A. Filoramo, W. Heller, G. Abstreiter, K. Brunner, G. Bohm, and G. Winmann, Phys. Rev. Lett. **76**, 3622 (1996).

[6] K. Chang and J.-B. Xia, Solid State Commun. **104**, 351 (1997).

[7] Y. Sugiyama, Y. Nakata, K. Imamura, S. Moto, and N. Yokoyama, Jpn. J. Appl. Phys., Part 1 **35**, 1320 (1996).

[8] Q. Xie, A. Madhukar, P. Chen, and N. P. Kobayashi, Phys. Rev. Lett. **75**, 2542 (1995).

[9] C. S. Lent, P. D. Tougaw, and W. Porod, Appl. Phys. Lett. **62**, 714 (1993).

[10] This method is inspired from the work of E. Kapon, D. M. Hang, and R. Bhat, Phys. Rev. Lett. **63**, 430 (1989).

[11] The ground-state energies are found by solving the time-dependent Schrödinger equation for an appropriately chosen initial state over a long time period t_f, and then calculating the approximate density of states, given by $\Gamma(E) = \int_0^{t_f} dt \, \langle \psi(z,0)\psi(z,t)\rangle e^{i2\pi Et/h}$.

[12] The effective masses and band offsets used in our calculations are based largely on parameters given in Y. Fu *et al.*, J. Appl. Phys. **83**, 1457 (1998).

[13] A similar result was obtained using a 3D pyramidal model in Ref. 6.

[14] M. Grundmann, O. Stier, and D. Bimberg, Phys. Rev. B **52**, 11 969 (1995); C. Pryor, M. E. Pystol, and L. Samuelson, *ibid.* **56**, 10 404 (1997).